Parallel-Stranded Guanine Quadruplex Interactions with a Copper Cationic Porphyrin†

Loryn R. Keating and Veronika A. Szalai*

Department of Chemistry and Biochemistry, University of Maryland, Baltimore County, 1000 Hilltop Circle, Baltimore, Maryland 21250

Received August 5, 2004; Revised Manuscript Received October 5, 2004

ABSTRACT: G-quadruplexes are formed by association of DNA strands containing multiple contiguous guanines. The capability of drugs to induce formation of or stabilize G-quadruplexes is an active area of investigation. We report the interactions of CuTMpyP4, the Cu^{2+} derivative of 5,10,15,20-tetrakis-(1-methyl-4-pyridyl)-21H,23H-porphine, with the parallel-stranded G-quadruplexes formed by $d(T_4G_4T_4)$ (**1**) and $d(T_4G_8T_4)$ (**3**). Absorption titrations of CuTMpyP4 with $(\mathbf{1})_4$ or $(\mathbf{3})_4$ cause both bathochromicity and hypochromicity of the porphyrin Soret band, with larger changes observed for the longer oligonucleotide. An approximate binding constant for $(\mathbf{1})_4$ and CuTMpyP4 according to the Scatchard model is $5.6 \times 10^6\ M^{-1}$ in terms of quadruplexes and according to the McGhee−von Hippel model is $1.3 \times 10^6\ M^{-1}$ in terms of potential binding sites. An approximate binding constant for $(\mathbf{3})_4$ and CuTMpyP4 according to the Scatchard model is $5.2 \times 10^7\ M^{-1}$ in terms of quadruplexes and in terms of the McGhee−von Hippel model is $2.4 \times 10^6\ M^{-1}$ in terms of potential binding sites. The site size for CuTMpyP4 and $(\mathbf{1})_4$ is four using the McGhee−von Hippel model. We find a 2:1 binding stoichiometry for CuTMpyP4 and $(\mathbf{1})_4$ and a 3:1 binding stoichiometry for CuTMpyP4 and $(\mathbf{3})_4$ using the method of continuous variation analysis. Induced emission spectra of CuTMpyP4 with $(\mathbf{1})_4$ or $(\mathbf{3})_4$ indicate a mode of binding in which the ligand is protected from the solvent. Electron paramagnetic resonance spectra of CuTMpyP4 with added oligonucleotide show an increase in the Cu−N superhyperfine coupling constant as the length of the oligonucleotide increases. On the basis of these data, we propose that for both $(\mathbf{1})_4$ and $(\mathbf{3})_4$, CuTMpyP4 molecules externally stack at each end of the run of guanines, similar to other planar G-quadruplex ligands. For $(\mathbf{3})_4$, our data are consistent with intercalation of a CuTMpyP4 molecule into the G-quadruplex.

Telomeric DNA is the noncoding DNA located at the end of linear eukaryotic chromosomes (*1*). The majority of telomeric DNA is double-stranded, but a significant portion of the 3′ end is single-stranded and guanine-rich (*2*). *In vitro*, the single-stranded guanine-rich portion of telomeres can form inter- or intramolecular quadruple helices, called G-quadruplexes (*2*, *3*). A guanine quartet is composed of a planar layer of four guanines, where each guanine accepts and donates two Hoogsteen hydrogen bonds (Figure 1A) (*4*). When the single-stranded 3′ end of a telomere folds into a G-quadruplex, it is no longer available to act as a primer for the enzyme telomerase (*3*). Telomerase is deactivated in most somatic cells at birth, but in 85−90% of human tumors, it acts to extend telomere length, thus rescuing cells from cell crisis (*2*). The potential application of G-quadruplexes to cancer treatment has been the driving force for investigation of ligands that stabilize G-quadruplexes and/or induce their formation (*3*−*18*).

The behavior of both inter- and intramolecular G-quadruplexes with planar, aromatic DNA-binding ligands has been investigated with G-quadruplexes containing three or four stacks of guanine quartets (*1*, *3*, *4*, *10*, *12*, *16*−*22*). The mode of ligand binding to G-quadruplexes is classified as end stacking, when a ligand binds to one face of a single guanine quartet in the G-quadruplex, intercalation, when a ligand binds between two guanine quartets in the G-quadruplex, or groove (external) binding (*9*, *18*). For the majority of ligand and G-quadruplex interactions investigated, end stacking predominates (*4*, *9*, *12*, *16*, *17*, *19*−*22*). The possibility of intercalation between guanine quartets in a G-quadruplex containing more than four sequential guanine stacks has not been investigated. The free-base porphyrin 5,10,15,20-tetrakis(1-methyl-4-pyridyl)-21H,23H-porphine (H_2TMpyP4),[1] which is similar in width to a guanine quartet, has been proposed to bind to G-quadruplexes both by end stacking and intercalation, although the existence of the latter binding mode is under dispute in the literature (*1*, *9*, *18*−*20*). The binding of H_2TMpyP4 to G-quadruplexes has been emphasized because this porphyrin stabilizes intramolecular G-quadruplexes and retards tumor growth, presumably through telomerase inhibition (*6*, *15*).

Unresolved issues relevant to the mode of action of free-base porphyrins in telomerase inhibition are the number and locations of porphyrins bound to G-quadruplexes. The binding of the free-base cationic porphyrin H_2TMpyP4 to the parallel-stranded G-quadruplex formed by $d(T_4G_4)$ has been investigated principally by two groups. Although the

† Supported by a grant from Research Corporation (RI1053).

* To whom correspondence should be addressed. E-mail: vszalai@umbc.edu. Phone: 410-455-1576. Fax: 410-455-2608.

[1] Abbreviations: H_2TMpyP4, 5,10,15,20-tetrakis(1-methyl-4-pyridyl)-21H,23H-porphine; CuTMpyP4, Cu^{2+} derivative of H_2TMpyP4; CD, circular dichroism; EPR, electron paramagnetic resonance; PIPER, *N*,*N*′-bis[2-(1-piperidino)ethyl]-3,4,9,10-perylenetetracarboxylic diimide.

10.1021/bi0483209 CCC: $27.50
Published on Web 11/24/2004

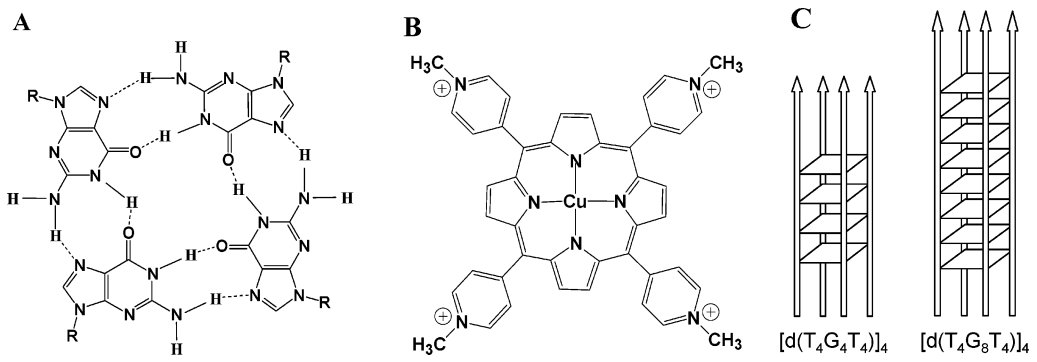

FIGURE 1: (A) Structure of a guanine quartet. (B) Structure of CuTMpyP4. (C) Sequences and schematic diagram of G-quadruplex-forming oligonucleotides **1** and **3**.

behavior of H_2TMpyP4 with the same G-quadruplex was investigated under different solution conditions, a similar 12−13 nm red shift and 40% hypochromicity of the Soret band of the porphyrin is reported (*1*, *18*). In contrast, the binding constants for H_2TMpyP4 and $[d(T_4G_4)]_4$ differ by almost 2 orders of magnitude: the binding constant (in terms of quadruplexes) determined by Haq et al. is 17×10^4 M^{-1} (*18*), while that reported by Anantha et al. is 2.7×10^7 M^{-1} (*1*). Using the method of continuous variation analysis, Haq et al. report a binding stoichiometry of three molecules of H_2TMpyP4 per mole of $[d(T_4G_4)]_4$ (*18*). By Scatchard analysis, Anantha et al. determined that the binding stoichiometry is one porphyrin per $[d(T_4G_4)]_4$ (*1*).

In contrast to the free-base porphyrin, the interactions of metalloporphyrins with G-quadruplexes have not been investigated intensively (*4*). Recently, it was discovered that the binding constant for H_2TMpyP4 with poly(rA)·poly(rU) or with poly(rA)·poly(dT) was increased when Cu^{2+} was inserted into the core of the porphyrin (*23*). We use CuTMpyP4, the Cu^{2+} derivative of H_2TMpyP4 (Figure 1B), because it does not have axial ligands, making its behavior similar to that of H_2TMpyP4, and like the free-base porphyrins, CuTMpyP4 is easy to monitor spectrophotometrically. Using CuTMpyP4 instead of H_2TMpyP4 has the advantage that both emission spectroscopy and electron paramagnetic resonance (EPR) spectroscopy can be used to discern the environment of the porphyrin when bound to G-quadruplexes. EPR spectra clearly show when two CuTMpyP4 molecules interact at distances of <4 Å (*24*, *25*). A further advantage to investigating the interactions of CuTMpyP4 instead of H_2TMpyP4 with G-quadruplexes is that, for porphyrin and duplex DNA systems with low porphyrin to base-pair ratios, the binding mode of CuTMpyP4 is less sensitive to changes in ionic strength than that of the free-base porphyrin (*26*). In addition to using a G-quadruplex with four guanine quartets, we have employed a G-quadruplex containing eight guanine quartets (Figure 1C) to test the hypothesis that a ligand can intercalate between guanine stacks if longer runs of guanines are available. Using a combination of UV−visible, emission, and EPR spectroscopies, we propose a model for the binding of CuTMpyP4 to the parallel-stranded G-quadruplexes formed by $d(T_4G_4T_4)$ and $d(T_4G_8T_4)$. In both cases, we propose that CuTMpyP4 end stacks between guanines and thymines on both the 3′ and 5′ sides of the G-quadruplexes. For $d(T_4G_8T_4)$, we propose that the third molecule of CuTMpyP4 intercalates between guanine quartets.

MATERIALS AND METHODS

Materials. Water was obtained from a Milli-Q Academic A10 system with a resistivity of 18.2 $M\Omega^{-1}$ and a total organic content of less than or equal to 34 ppb. H_2TMpyP4 (tetra-*p*-tosylate salt) was purchased from Aldrich (Milwaukee, WI). The copper derivative of H_2TMpyP4 (CuTMpyP4) was synthesized according to the procedure of Pasternack et al. (*27*). CuTMpyP4 solutions in H_2O were stored in the dark to prevent photodegradation. Herring-testes DNA was purchased from Sigma Chemical Company (St. Louis, MO) and was suspended in water prior to use. Mono- and dibasic potassium phosphate and glycerol were purchased from Fisher Scientific (NJ), and potassium chloride was purchased from Acros.

The oligonucleotides $d(T_4G_4T_4)$ (**1**), $d(A_4C_4A_4)$ (**2**), $d(T_4G_8T_4)$ (**3**), and $d(A_4C_8A_4)$ (**4**) were purchased from the W. M. Keck Facility (Yale University, New Haven, CT). They were resuspended in water and stored at −13 °C. Denaturing polyacrylamide gels were run of a sample of each oligonucleotide to ensure strand-length homogeneity (*28*). The concentration of each oligonucleotide was determined by measuring its absorbance at 260 nm using the following extinction coefficients: herring-testes DNA = 6600 M^{-1} cm^{-1} (*28*), **1** = 106.4 mM^{-1} cm^{-1}, **2** = 128.6 mM^{-1} cm^{-1}, **3** = 146.8 mM^{-1} cm^{-1}, and **4** = 157.4 mM^{-1} cm^{-1}. Concentrations of oligonucleotides (single-stranded or G-quadruplex) are per strand unless stated otherwise. Extinction coefficients for the oligonucleotides were calculated by the nearest neighbor method (*29*).

Circular Dichroism (CD). CD experiments were performed at room temperature using a Jasco J-710 spectropolarimeter coupled to a 486 personal computer for data collection. A quartz cuvette with a 0.1 cm path length was used for all CD experiments. Each spectrum collected was an average of three scans. In addition, the spectrum of the corresponding buffer was collected and subtracted from that of the sample.

Solutions containing 40.7 μM **1**, 40.7 μM **1** plus 34.8 μM CuTMpyP4, 40.7 μM **1** plus 40.3 μM **2**, 42.8 μM **3**, 42.8 μM **3** plus 46.4 μM CuTMpyP4, and 42.8 μM **3** plus 42.6 μM **4** each in 10 mM KP_i and 49 mM KCl at pH 7.0 were prepared for CD analysis. Each sample was heated to 95 °C for 10 min and slowly cooled to room temperature over 2−3 h. A CD spectrum of 50 μM herring-testes DNA in 50 mM NaP_i at pH 7.0 also was collected.

UV−Vis Absorbance Titration Experiments. Absorption spectra were collected at room temperature using a Jasco

V-560 UV−vis double beam spectrophotometer connected to a Dell Celeron computer for data collection. Methacrylate cuvettes with a 1 cm path length were used for all absorbance studies; the reference solution was 10 mM KP_i and 50 mM KCl at pH 7.1.

All absorption titrations were performed by adding a stock solution of oligonucleotide in 10 mM KP_i and 50 mM KCl at pH 7.1 to a cuvette containing approximately 1 μM CuTMpyP4 in 10 mM KP_i and 50 mM KCl at pH 7.1. All solutions were prepared either on the day of the titration or on the day before the titration. Oligonucleotide solutions were stored overnight at 4 °C, and porphyrin solutions were stored in the dark at room temperature. The concentration of CuTMpyP4 at the beginning of a titration was determined by measuring its absorbance at 425 nm and using the extinction coefficient for free CuTMpyP4 of $2.31 \times 10^5\ M^{-1}\ cm^{-1}$ (*27*).

Spectra were collected from 350 to 800 nm to monitor the position of the absorbance bands of CuTMpyP4. The titration was terminated when the wavelength of the CuTMpyP4 Soret band ceased to shift upon five successive additions of oligonucleotide. Multiple titrations were performed for **1** and **3** to give average extinction coefficients for bound CuTMpyP4.

The total CuTMpyP4 concentration was corrected for dilution effects ($[CuTMpyP4]_{corrected}$) resulting from the change in volume incurred by the addition of oligonucleotide. The fraction of CuTMpyP4 bound (α) was found using eq 1 (*30*) where Abs $CuTMpyP4_{free}$ is the absorbance of the

$$\alpha = (\text{Abs CuTMpyP4}_{free} - \text{Abs}_{mix})/(\text{Abs CuTMpyP4}_{free} - \text{Abs CuTMpyP4}_{bound}) \quad (1)$$

porphyrin in the absence of oligonucleotide, Abs_{mix} is the absorbance at any given point during the titration, and Abs $CuTMpyP4_{bound}$ is the absorbance of the fully bound porphyrin as measured at the Soret maximum of free porphyrin (425 nm). Equations 2 and 3 were applied to calculate the concentration of free CuTMpyP4 ($[CuTMpyP4]_{free}$) and the concentration of bound CuTMpyP4 ($[CuTMpyP4]_{bound}$).

$$[CuTMpyP4]_{free} = [CuTMpyP4]_{corrected}(1 - \alpha) \quad (2)$$

$$[CuTMpyP4]_{bound} = [CuTMpyP4]_{corrected} - [CuTMpyP4]_{free} \quad (3)$$

The extinction coefficient for the bound porphyrin (ϵ_{bound}) was found from eq 4 and ϵ_{bound} was used subsequently to

$$\epsilon_{bound} = \text{Abs CuTMpyP4}_{bound}/[CuTMpyP4]_{bound} \quad (4)$$

determine the % hypochromicity of the Soret band of the porphyrin (eq 5).

$$\%\ \text{hypochromicity} = [(\epsilon_{free} - \epsilon_{bound})/\epsilon_{free}] \times 100 \quad (5)$$

Continuous Variation Analysis. Stock solutions of 30 μM CuTMpyP4, 30 μM $(\mathbf{1})_4$ in terms of quadruplexes, and 30 μM $(\mathbf{3})_4$ in terms of quadruplexes were prepared in 10 mM KP_i and 50 mM KCl at pH 7.1. Three series of solutions were used for the experiments: one with varying mole fractions of CuTMpyP4 and $(\mathbf{1})_4$, one with varying mole fractions of CuTMpyP4 and $(\mathbf{3})_4$, and one with varying concentrations of CuTMpyP4. The sum of the porphyrin and quadruplex concentrations was always 30 μM.

Absorbance difference spectra were collected from 350 to 800 nm with 0.1 cm path-length quartz cuvettes. For each spectrum collected, the CuTMpyP4 solution without oligonucleotide was placed in the reference compartment and the corresponding CuTMpyP4 solution with oligonucleotide was placed in the sample compartment. Cuvettes were washed with 10% HCl between measurements on solutions containing greater than a CuTMpyP4 mole fraction of 0.7 because the porphyrin adsorbs to quartz (*18*).

The difference in the absorbance values at two wavelengths was plotted versus the CuTMpyP4 mole fraction to generate a Job plot. The wavelengths were 444 and 420 nm or 446 and 422 nm for $(\mathbf{1})_4$ and $(\mathbf{3})_4$, respectively. Data points for a CuTMpyP4 mole fraction of 0.95 with $(\mathbf{3})_4$ and CuTMpyP4 mole fractions of 0.9 and 0.95 with $(\mathbf{1})_4$ were omitted because of aggregation at these high porphyrin mole fractions. Linear regression analysis of the data was performed in Microsoft Excel.

Emission Spectroscopy. Emission spectra were collected at room temperature using a Jobin−Yvon−Spex FluoroMax-2 fluorimeter. A 1 cm path-length quartz cuvette was used for all experiments. Emission spectra were collected for 5 μM CuTMpyP4, 5 μM CuTMpyP4 with 24 μM $(\mathbf{1})_4$, and 5 μM CuTMpyP4 with 24 μM $(\mathbf{3})_4$. The excitation wavelength was 434 nm, and the emission spectrum was collected from 650 to 850 nm. The 434 nm excitation wavelength corresponds to the absorption maximum for porphyrin fully bound to $(\mathbf{1})_4$. Use of 437 nm [i.e., the absorption maximum for porphyrin fully bound to $(\mathbf{3})_4$] instead of 434 nm as the excitation wavelength for CuTMpyP4 with $(\mathbf{3})_4$ produced an identical emission spectrum (data not shown). Therefore, the excitation wavelength corresponding to the absorption maximum of porphyrin fully bound to $(\mathbf{1})_4$ was used because the absorption titrations do not show tight isobestic points and because only end-stacked or intercalated CuTMpyP4 emits. Each spectrum is a sum of four scans collected with an integration time of 0.5 s, an excitation slit width of 3 nm, and an emission slit width of 7 nm.

EPR Spectroscopy. EPR spectra were collected on a Bruker EMX 6/1 X-band spectrometer equipped with an Oxford Instruments ESR900 liquid He cryostat. Instrumental parameters were the following: $T = 20$ K, microwave frequency = 9.37 GHz, microwave power = 0.5 mW, modulation amplitude = 5 G, gain = 5×10^4, time constant = 81.92 ms, conversion time = 81.92 ms, and number of scans = 8. Spectra were collected for 200 μL solutions containing final concentrations of 50 μM CuTMpyP4, 50 μM CuTMpyP4 plus 300 μM $(\mathbf{1})_4$, or 50 μM CuTMpyP4 plus 500 μM $(\mathbf{3})_4$ each in 10 mM KP_i and 50 mM KCl at pH 7.1 with 50% glycerol (v/v). Glycerol is added as a cryoprotectant and also because it eliminates spectral contributions from dimeric porphyrin species formed in solution (*31*). EPR spectra also were collected for a duplicate set of samples only differing in that they had equimolar concentrations of $(\mathbf{1})_4$ or $(\mathbf{3})_4$. The spectra are identical to those collected for the samples described above (data not shown).

Table 1: CD Parameters for CuTMpyP4 with DNA

nucleic acid	[nucleic acid] (μM)[a]	[CuTMpyP4] (μM)	negative CD band (nm)	positive CD band (nm)
herring-testes DNA	50		246	276
1	41		245	269
1	41	35	245	269
ds(**1**:**2**)	41		249	276
3	43		242	264
3	43	46	242	264
ds(**3**:**4**)	43		244	276

[a] Nucleic acid concentration is in strands for oligonucleotides and in nucleotide phosphates for herring-testes DNA.

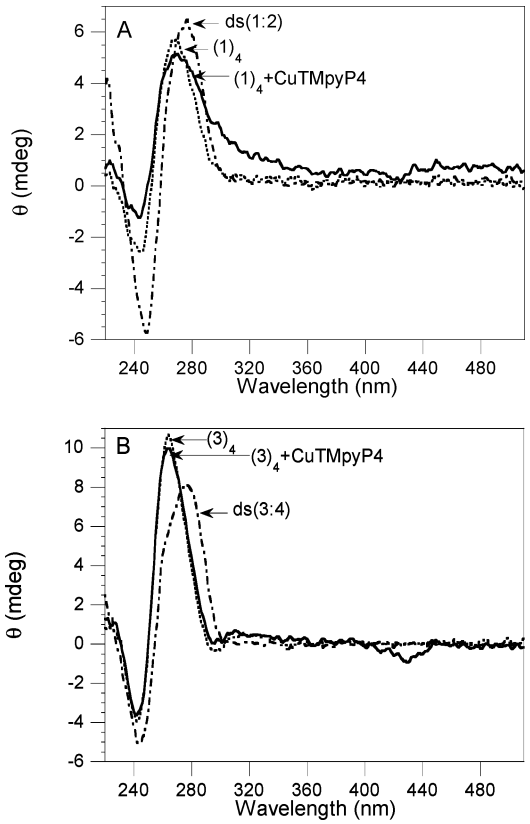

FIGURE 2: CD spectra of annealed G-quadruplex-forming oligonucleotides **1** and **3** in 10 mM KP_i and 49 mM KCl at pH 7.0. (A) $(\mathbf{1})_4$ contains 41 μM strand; ds(**1**:**2**) contains 41 μM **1** and 40 μM **2** (the Watson−Crick complement of **1**); and $(\mathbf{1})_4$ + CuTMpyP4 contains 41 μM $(\mathbf{1})_4$ and 35 μM CuTMpyP4. (B) $(\mathbf{3})_4$ contains 43 μM strand; ds(**3**:**4**) contains 43 μM **3** and 43 μM **4** (the Watson−Crick complement of **3**); and $(\mathbf{3})_4$ + CuTMpyP4 contains 43 μM $(\mathbf{3})_4$ and 46 μM CuTMpyP4.

RESULTS

CD. The CD spectra of annealed **1** and annealed **3** both display a positive CD band near 260 nm and a negative CD band near 240 nm, characteristic of parallel-stranded G-quadruplexes (*32*). The addition of CuTMpyP4 to **1** or **3** did not affect the position of the positive bands at 269 and 264 nm, respectively, or the position of the negative bands at 245 and 242 nm, respectively (Table 1 and Figure 2). For **1**, the positive 269 nm band was broader in the presence of CuTMpyP4 than in the absence of CuTMpyP4. In contrast to **1**, the overall shape of the CD spectrum for **3** did not change in the presence of CuTMpyP4. However, an induced CD band for CuTMpyP4 appeared at 429 nm. Upon binding to its Watson−Crick complement (**2**), the CD spectrum for

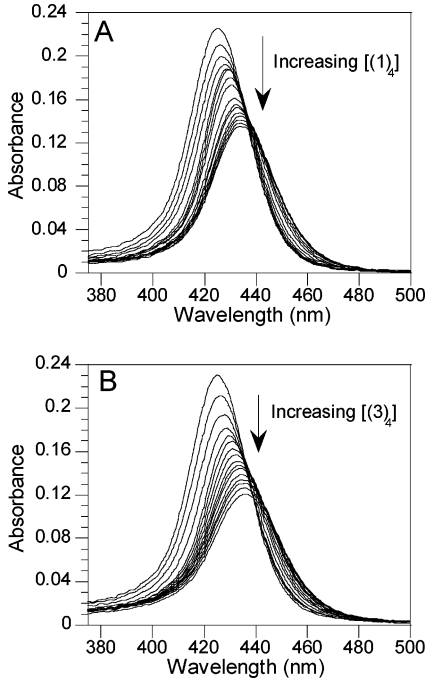

FIGURE 3: Absorbance spectra of 1 μM CuTMpyP4 with oligonucleotide (A) **1** or (B) **3** in 10 mM KP_i and 50 mM KCl at pH 7.1. Additions range from 0 to 10 μM strand for **1** and from 0 to 9 μM strand for **3**.

1 changed to give the characteristic CD spectrum for B-form duplex DNA (*29*, *33*). Similar shifts were observed for **3** after annealing to its Watson−Crick complement (**4**).

The ability of **1** or **3** in 10 mM KP_i buffer containing 50 mM KCl to form a G-quadruplex at room temperature was investigated. The CD spectra (not shown) collected for **1** or **3** in 10 mM KP_i and 50 mM KCl at pH 7.1 before and after annealing are nearly identical. Therefore, both oligonucleotides form parallel-stranded G-quadruplexes at room temperature, indicating that **1** and **3** do not need to be annealed to form a G-quadruplex prior to absorbance titrations when they are in 10 mM KP_i and 50 mM KCl.

UV−Vis Absorption. To ensure that the CuTMpyP4/oligonucleotide system was at equilibrium, an absorbance titration was performed by collecting two spectra after each oligonucleotide addition: the first spectrum was collected immediately after adding oligonucleotide, and the second was collected 10 min after adding oligonucleotide. No difference was observed for the red shift or hypochromicity of the CuTMpyP4 Soret band (data not shown) with and without the wait time, demonstrating that the system reached equilibrium during the 2−3 min between oligonucleotide addition, mixing, and spectral collection.

Absorbance spectra from the titrations of CuTMpyP4 with $(\mathbf{1})_4$ or $(\mathbf{3})_4$ are shown in Figure 3 and from the titrations of CuTMpyP4 with **2** or **4**, the Watson−Crick complements of **1** and **3**, are given in the Supporting Information. Table 2 shows a summary of the results for the titrations of CuTMpyP4 with $(\mathbf{1})_4$, **2**, $(\mathbf{3})_4$, or **4**. The largest red shift (12 nm) of the CuTMpyP4 Soret band was induced by binding to $(\mathbf{3})_4$, with the next largest red shift for binding to $(\mathbf{1})_4$. Smaller red shifts were observed for titrations of CuTMpyP4 with **2** and **4**. The binding of CuTMpyP4 to $(\mathbf{3})_4$ resulted in a higher hypochromicity of the CuTMpyP4 Soret band than the binding of CuTMpyP4 to $(\mathbf{1})_4$.

Table 2: Absorbance Titration Parameters for CuTMpyP4 with Oligonucleotides

oligonucleotide	[CuTMpyP4] (μM)	[oligonucleotide][a] (μM)	Soret band shift (nm)	% hypochromicity[b]
$(\mathbf{1})_4$	0.978	9.8	9	50
2	0.965	9.3	5	25
$(\mathbf{3})_4$	0.996	12.6	12	58
4	0.996	7.5	6	27

[a] Oligonucleotide strand concentration. [b] Soret band hypochromicity calculated using the average extinction coefficient for bound CuTMpyP4 derived from multiple titrations of $(\mathbf{1})_4$, $\epsilon_{bound} = 1.16 \pm 0.03 \times 10^5$ M^{-1}, and $(\mathbf{3})_4$, $\epsilon_{bound} = 9.98 \pm 0.67 \times 10^4$ M^{-1}; see eq 5 in the Materials and Methods.

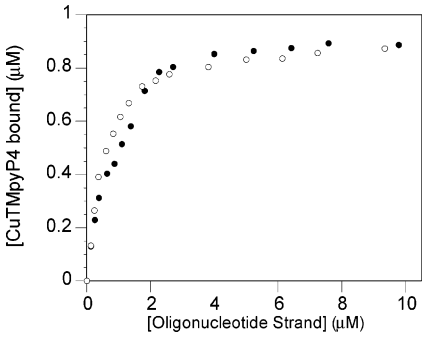

FIGURE 4: Binding curves for CuTMpyP4 with $(\mathbf{1})_4$ (●) or $(\mathbf{3})_4$ (○). $[CuTMpyP4]_{bound}$ was calculated as described in the Materials and Methods.

Binding curves for CuTMpyP4 with $(\mathbf{1})_4$ or $(\mathbf{3})_4$ plateau at approximately the same concentration of added oligonucleotide (Figure 4). It is important to remember that the binding curves shown in Figure 4 cannot be used to determine the number of CuTMpyP4 molecules bound per mole of G-quadruplex because the nucleic acid lattice containing the potential binding sites was titrated into a solution of the ligand (*34*). In other words, the final concentration of bound CuTMpyP4 depends on the total concentration of CuTMpyP4 so that the position of the binding curve plateau is not indicative of saturation of lattice binding sites. Instead, data must be analyzed using an appropriate binding model.

The Scatchard binding model determines the number(s) of equivalent binding sites and the affinities of ligands for those sites (*1*, *35*, *36*). Data from each absorbance titration were cast into Scatchard plots, $r/[CuTMpyP4]_{free}$ versus r. In our Scatchard analysis, r is the number of moles of bound CuTMpyP4 per mole of quadruplex. The Scatchard plots for the titrations of CuTMpyP4 with $(\mathbf{1})_4$ or $(\mathbf{3})_4$ are shown in Figure 5, and a similar analysis for CuTMpyP4 with **2** or **4** is given in the Supporting Information. None of the Scatchard plots is linear.

In an attempt to determine a binding constant, K_a, for CuTMpyP4 in terms of quadruplexes, data points between $r = 0.6$ and 2 for $(\mathbf{1})_4$ and between $r = 0.3$ and 0.54 for $(\mathbf{3})_4$ were fit to the Scatchard model using the computer program NFIT (*37*). The fit gave approximate K_a values of 5.6×10^6 and 5.2×10^7 M^{-1} for CuTMpyP4 with $(\mathbf{1})_4$ or $(\mathbf{3})_4$, respectively.

Another method to determine association constants for ligands binding to macromolecules containing multiple potential binding sites is application of the McGhee−von Hippel model (*38*). McGhee−von Hippel plots were generated for the absorbance titration data by redefining r as moles of bound CuTMpyP4 per mole of potential binding sites on $(\mathbf{1})_4$ or $(\mathbf{3})_4$. We assumed that the number of potential binding sites corresponded to the oligonucleotide length. Thus, the number of potential binding sites for $(\mathbf{1})_4$ and $(\mathbf{3})_4$ were 12 and 16, respectively. The McGhee−von Hippel plots have the same shape as the corresponding Scatchard plots. When NFIT and the McGhee−von Hippel model assuming noncooperative binding were used to determine binding constants, an approximate K_a for CuTMpyP4 and $(\mathbf{1})_4$ was determined to be 1.3×10^6 M^{-1} and an approximate K_a for CuTMpyP4 and $(\mathbf{3})_4$ was determined to be 2.4×10^6 M^{-1}, both in terms of potential binding sites.

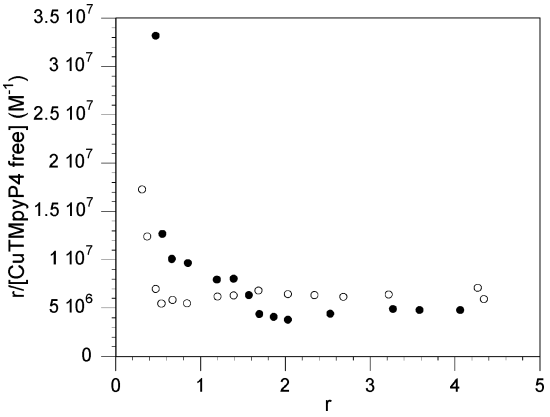

FIGURE 5: Scatchard plots for CuTMpyP4 with $(\mathbf{1})_4$ (●) or $(\mathbf{3})_4$ (○). r is moles of bound CuTMpyP4 per mole of quadruplex.

Chaires has suggested that for ligands binding to oligonucleotides in multiple equivalent, noninteracting sites, the appropriate expression to determine the binding constant and binding stoichiometry is eq 6 (*39*) where r is moles of bound

$$r = (nK[\text{ligand}]_{free})/(1 + K[\text{ligand}]_{free}) \qquad (6)$$

ligand (CuTMpyP4) per mole of macromolecule (G-quadruplex), K is the association constant, and n is the number of ligand-binding sites on the macromolecule (*39*). Rearrangement of eq 6 yields the standard equation used for Scatchard analysis. A plot of r versus free ligand concentration should yield a parabolic plot that can be fit with eq 6 to obtain the number of ligand-binding sites and the association constant of the ligand for DNA. Our plots of r (in terms of quadruplexes) versus free CuTMpyP4 concentration (Figure 6) from the absorbance titrations of CuTMpyP4 with $(\mathbf{1})_4$ or $(\mathbf{3})_4$ are sigmoidal, with the plot for the titration of CuTMpyP4 with $(\mathbf{1})_4$ showing the most sigmoidal curvature. The sigmoidal shape of both plots indicates that the binding of CuTMpyP4 to $(\mathbf{1})_4$ or $(\mathbf{3})_4$ is cooperative (*36*, *40*) and means that eq 6 is not sufficient to evaluate binding of CuTMpyP4 to $(\mathbf{1})_4$ or $(\mathbf{3})_4$. As a result of the observed cooperativity, NFIT and the McGhee−von Hippel equation accounting for cooperative behavior were used to fit the data. This model yielded a binding constant of 1.2×10^6 M^{-1} for CuTMpyP4 with $(\mathbf{1})_4$ in terms of potential binding sites; however, use of the model to determine the binding constant for CuTMpyP4 with $(\mathbf{3})_4$ was unsuccessful.

Continuous Variation Analysis. The method of continuous variation analysis (Job plot) was used to determine the number of molecules of CuTMpyP4 binding per quadruplex (Figure 7). The difference spectra used to generate the Job

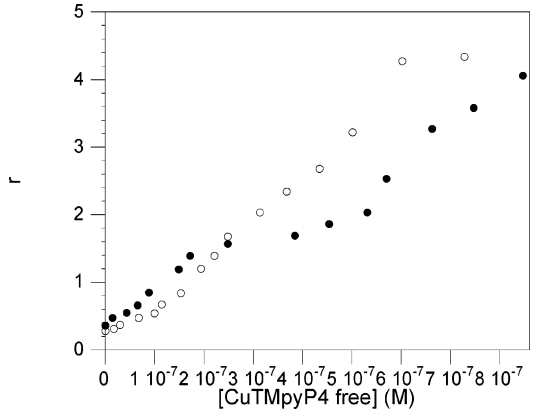

FIGURE 6: Plots of r (moles of bound CuTMpyP4 per mole of quadruplex) versus $[CuTMpyP4]_{free}$ for the absorbance titrations of CuTMpyP4 with $(\mathbf{1})_4$ (●) or $(\mathbf{3})_4$ (○).

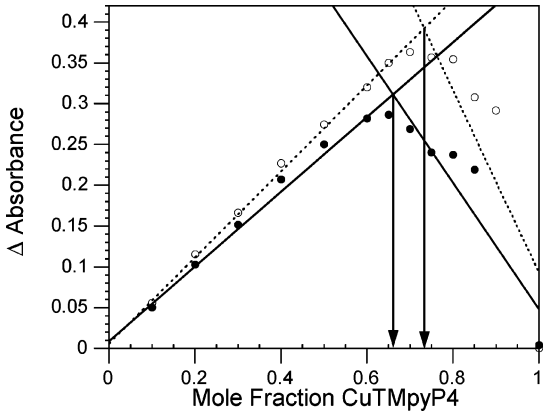

FIGURE 7: Job plots resulting from the method of continuous variation analysis for (A) CuTMpyP4 with $(\mathbf{1})_4$ and (B) CuTMpyP4 with $(\mathbf{3})_4$.

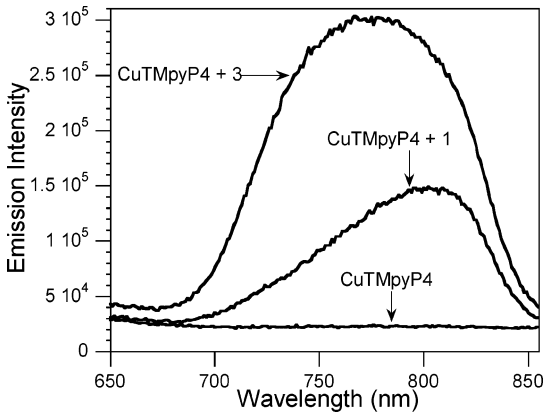

FIGURE 8: Emission spectra (λ_{ex} = 434 nm) of 5 μM CuTMpyP4, 5 μM CuTMpyP4 with 24 μM $(\mathbf{1})_4$, or 5 μM CuTMpyP4 with 24 μM $(\mathbf{3})_4$. All solutions contain 10 mM KP_i and 50 mM KCl at pH 7.1.

plots in Figure 7 are in the Supporting Information. The point of intersection of the two best fit lines for the Job plot for CuTMpyP4 and $(\mathbf{1})_4$ is 0.66, giving a binding stoichiometry of 2 mol of CuTMpyP4/mol of $(\mathbf{1})_4$. The point of intersection of the two best fit lines for the Job plot for CuTMpyP4 and $(\mathbf{3})_4$ is 0.73, yielding a binding stoichiometry of 3 mol of CuTMpyP4/mol of $(\mathbf{3})_4$.

Emission Spectra. As shown in Figure 8, solutions containing CuTMpyP4 and oligonucleotide displayed emission spectra between 690 and 850 nm when excited at a

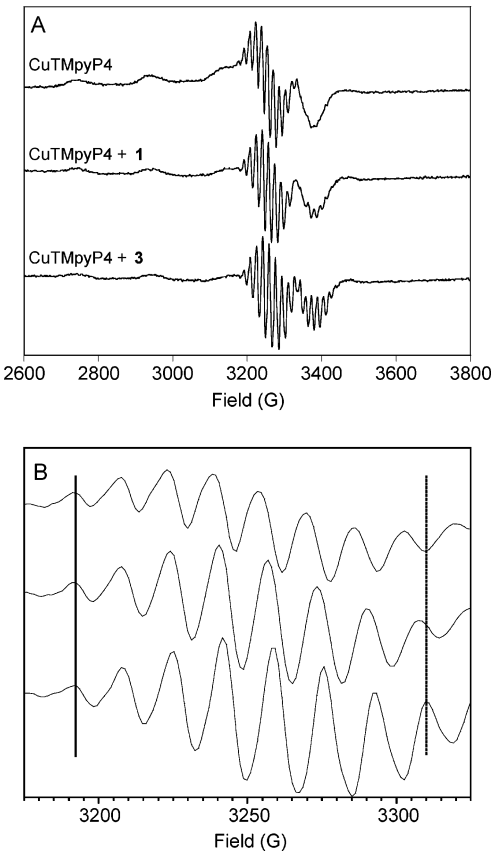

FIGURE 9: X-band EPR spectra (20 K) of 50 μM CuTMpyP4 in the presence or absence of 300 μM **1** or 500 μM **3**. (A) Unscaled and (B) expanded spectra showing the increase in the average Cu−N superhyperfine coupling constant as a function of added oligonucleotide. Spectra are in the same order as in A. The vertical line at low field shows that the superhyperfine peaks are aligned in all spectra. The vertical line at approximately 3340 G illustrates the lack of alignment of the superhyperfine peaks at high field. Spectra were scaled so that the lowest field peaks are the same intensity. EPR instrumental conditions are in the Materials and Methods.

wavelength of 434 nm. The corresponding CuTMpyP4 solution without oligonucleotide did not emit under the same experimental conditions. CuTMpyP4 with $(\mathbf{3})_4$ has an emission intensity peak at 785 nm, and its emission spectrum is symmetrical. In contrast, CuTMpyP4 bound to $(\mathbf{1})_4$ has an emission maximum at 805 nm, and its spectrum is less symmetrical than that displayed by CuTMpyP4 with $(\mathbf{3})_4$. When all of the CuTMpyP4 is bound (i.e., when a large excess of G-quadruplex is present), the emission intensity of CuTMpyP4 with $(\mathbf{3})_4$ is about twice as large as that for CuTMpyP4 with $(\mathbf{1})_4$. The 2-fold observed difference in emission intensity is not due to the difference in absorptivity of CuTMpyP4 bound to $(\mathbf{3})_4$ versus $(\mathbf{1})_4$ at 434 nm because that ratio is 1.4 [%T for 5 μM CuTMpyP4 with $(\mathbf{3})_4$ at 434 nm is 28%, and %T for 5 μM CuTMpyP4 with $(\mathbf{1})_4$ at 434 nm is 20%].

EPR Spectroscopy. Low-temperature spectra of CuTMpyP4 show increased resolution in the high-field region of the spectrum in the presence of oligonucleotide (Figure 9). The main features in EPR spectra of monomeric Cu^{2+} porphyrins arise from hyperfine coupling between the unpaired electron on Cu^{2+} and the $^{63,65}Cu$ ($I = {}^3/_2$) nucleus and from superhyperfine coupling with ^{14}N ($I = 1$) atoms of the porphyrin (*24*, *41*). The spectra in Figure 9 have $A_{||}$

values of 199.4 ± 4.7, 201.2 ± 3.0, and 202.9 ± 4.6 G for free CuTMpyP4, CuTMpyP4 with $(\mathbf{1})_4$, and CuTMpyP4 with $(\mathbf{3})_4$, respectively. The $g_{||}$ values decrease from 2.209 for free CuTMpyP4, to 2.203 for CuTMpyP4 with $(\mathbf{1})_4$, to 2.199 for CuTMpyP4 with $(\mathbf{3})_4$. For CuTMpyP4 in buffer solution, our $A_{||}$ value compares well to a published $A_{||}$ value of 213.4 G (598 MHz) and the $g_{||}$ value exactly matches that reported for CuTMpyP4 in a 1:1 (v/v) mixture of water/dimethyl sulfoxide at 4 K (*42*). The $A_{||}$ values for CuTMpyP4 bound to $(\mathbf{1})_4$ or $(\mathbf{3})_4$ are slightly smaller, and the $g_{||}$ values are slightly higher than those reported for CuTMpyP4 bound to long strands of random-sequence DNA (*31*, *43*, *44*). The average nitrogen hyperfine coupling constant (A_N) increases from 15.8 ± 0.62 for CuTMpyP4 in buffer to 16.4 ± 0.04 and 16.9 ± 0.64 for CuTMpyP4 with $(\mathbf{1})_4$ and $(\mathbf{3})_4$, respectively (Figure 9B). These nitrogen hyperfine coupling constants are very similar to those used for spectral simulations of CuTMpyP4 bound to calf thymus DNA in gels and published previously (*43*).

DISCUSSION

Interaction of CuTMpyP4 with $(\mathbf{1})_4$ and $(\mathbf{3})_4$. The oligonucleotides used in our study form parallel-stranded G-quadruplexes in 10 mM KP_i and 50 mM KCl, as expected based on the similarity of these oligonucleotides to other sequences that form parallel-stranded G-quadruplexes (*8*, *17*, *45*−*47*). As observed for other DNA-binding ligands and G-quadruplexes, binding of CuTMpyP4 to $(\mathbf{1})_4$ or $(\mathbf{3})_4$ is rapid and does not disrupt the G-quadruplex structure (*1*, *3*, *12*, *17*−*19*, *48*).

A characteristic of porphyrin−DNA systems is that intercalative binding results in a ≥15 nm red shift and a ≥35% hypochromicity of the porphyrin Soret band. A negative-induced CD band at a wavelength corresponding to the porphyrin Soret region is observed also. External binding results in a ≤8 nm red shift and either hyperchromicity or ≤10% hypochromicity of the porphyrin Soret band. In this case, a positive-induced CD band at a wavelength corresponding to the porphyrin Soret region is observed (*26*, *27*, *49*). For the titrations of CuTMPyP4 with $(\mathbf{1})_4$ or $(\mathbf{3})_4$, the Soret band red shifts by 9−12 nm and displays a hypochromicity of ≥50%. These red shifts do not fall in the range for either external or intercalative binding, but the large hypochromicities signal intercalation. It is important to remember that the red shifts and hypochromicities given above for different binding modes were determined for long pieces of duplex DNA, where end stacking is insignificant. As a result, a conclusion as to the binding mode of CuTMpyP4 to $(\mathbf{1})_4$ or $(\mathbf{3})_4$ cannot be made from absorbance measurements alone. The fact that the CD spectrum for CuTMpyP4 with $(\mathbf{3})_4$ contains a negative-induced CD band in the CuTMpyP4 Soret region indicates intercalation of the porphyrin into this G-quadruplex assuming that conclusions regarding CD bands of CuTMpyP4 with B-form DNA (*27*) can be applied to G-quadruplexes, an assumption that may or may not be valid.

The guanine−cytosine (G−C) content of the DNA also plays a role in the electronic spectroscopy of porphyrins bound to DNA. Pasternack and co-workers have shown that with calf thymus DNA, poly(dG−dC), and poly(dA−dT), the % hypochromicity and red shift of the Soret band of either H_2TMpyP4 or CuTMpyP4 increase as the G−C content of the nucleic acid increases (*27*). We observe a similar trend for the absorbance titrations of CuTMpyP4 with $(\mathbf{1})_4$ or $(\mathbf{3})_4$ (Table 2). Oligonucleotides **1** and **3** contain 33 and 50% guanine, respectively, and the red shift and the hypochromicity of the CuTMpyP4 Soret band both increase with the corresponding increase in the guanine content of the oligonucleotide. On the other hand, absorbance titrations of CuTMpyP4 with **2** (33% cytosine) show the same magnitude red shift and hypochromicity of the CuTMpyP4 Soret band as titrations with **4** (50% cytosine). Therefore, it appears that the DNA guanine content and not the cytosine content controls the magnitude of the red shift and hypochromicity of the CuTMpyP4 Soret band. This conclusion implies that the type of binding of porphyrins to GC sites in random sequence DNA is similar to that for porphyrins binding to G-quadruplexes.

While the free-base and Cu^{2+} forms of TMpyP4 are similar in their interactions with DNA, they do not display identical behavior in all instances. The CuTMpyP4 Soret band red shift and hypochromicity are smaller than those for the H_2-TMpyP4 Soret band in titrations with calf thymus DNA, poly(dG−dC), or poly(dA−dT) (*27*). We observe a smaller red shift of the CuTMpyP4 Soret band with $(\mathbf{1})_4$ compared to the H_2TMpyP4 Soret band red shift observed by Haq et al. (*18*) and Anantha et al. (*1*) for titrations of H_2TMpyP4 with $[d(T_4G_4)]_4$ [a quadruplex similar to $(\mathbf{1})_4$]. However, the CuTMpyP4 Soret band exhibits a larger % hypochromicity with $(\mathbf{1})_4$ than Haq et al. (*18*) and Anantha et al. (*1*) observed for the H_2TMpyP4 Soret band with $[d(T_4G_4)]_4$. The larger % hypochromicity could be due to the fact the ionic strength of our buffer is lower than that used by either Haq et al. or Anantha et al. (*1*, *18*). A decrease in hypochromicity has been reported for both H_2TMpyP4 and CuTMpyP4 binding to calf thymus DNA as ionic strength increases, with a significantly smaller decrease observed for CuTMpyP4 as compared to H_2TMpyP4 (*43*).

To determine binding stoichiometry using the method of continuous variation analysis, the reactant concentration sum must be much greater than the dissociation constant, requiring at least an approximate value for K_a (*50*). We obtained K_a by analyzing absorption titration data for CuTMpyP4 with $(\mathbf{1})_4$ using either the Scatchard or McGhee−von Hippel models. The literature on the applicability of the method of continuous variation analysis to ligand binding to macromolecules is inconsistent. According to Chaires, this method can be used to evaluate stoichiometry independent of the assumed binding model (*39*). Ingham (*51*), as cited by Nakatani et al. (*14*), states that the method of continuous variation analysis can be used only to determine the binding stoichiometry for ligand binding to independent equivalent sites; however, no theoretical or experimental evidence was offered to support this statement (*51*). In contrast, Huang mathematically demonstrated that the method of continuous variation analysis is applicable for cooperative ligand binding with the exception of the case where the ligand binds to a single macromolecular conformation (*52*).

By Scatchard analysis, the approximate binding constant for CuTMpyP4 and $(\mathbf{1})_4$ is approximately 2-fold smaller than that determined by Anantha et al. (*1*) by Scatchard analysis for H_2TMpyP4 with $[d(T_4G_4)]_4$. This similarity in binding constants coincides with the previously reported similarity

in the binding constants for CuTMpyP4 ($K_a = 8 \times 10^5\ M^{-1}$) and H_2TMpyP4 ($K_a = 7.7 \times 10^5\ M^{-1}$) with poly(dG−dC) (*27*). The binding constant that we determined for CuTMpyP4 with $(\mathbf{1})_4$ using the McGhee−von Hippel model is an order of magnitude smaller than the one we obtained using the Scatchard model. This result is logical because the Scatchard equation calculates the binding constant in terms of quadruplexes, whereas the McGhee−von Hippel equation calculates the binding constant in terms of potential binding sites per quadruplex.

Scatchard plots are linear only for ligand binding to independent and equivalent sites, with any curvature being due to the existence of more than one type of binding site, ligand−ligand interactions, or neighbor-exclusion effects (*38*). When ligand binding exhibits any of the latter three behaviors, Scatchard analysis cannot be used to determine binding constants accurately (*38*). The fact that we observe cooperativity means that the binding constants that we determined by fitting only the linear portion of the Scatchard plot for CuTMpyP4 with $(\mathbf{1})_4$ or $(\mathbf{3})_4$ are approximate. The McGhee−von Hippel equation accounts for neighbor-exclusion effects and a modified form of the McGhee−von Hippel equation accounts for cooperative binding. Because ligand binding to long sequences of DNA is subject to neighbor-exclusion effects, binding constants determined using the McGhee−von Hippel equation are more accurate than values determined by Scatchard analysis. It is important to remember that the McGhee−von Hippel model was derived for an infinitely long homogeneous lattice, a condition oligonucleotides do not satisfy (*39*). For the method of continuous variation analysis, we accounted for the shortcomings in both the Scatchard and McGhee−von Hippel models by using a total reactant concentration that was much greater than the smallest dissociation constant determined by either model.

Binding Mode of CuTMpyP4 with $(\mathbf{1})_4$ and $(\mathbf{3})_4$. Although crystal structures of $(\mathbf{1})_4$ and $(\mathbf{3})_4$ are not available to guide us in developing a model for CuTMpyP4 binding, our spectroscopic information can be combined with the available structures of other parallel-stranded G-quadruplexes to generate a model. Crystal structures of $[d(TG_4T)]_4$, a G-quadruplex similar to $(\mathbf{1})_4$, show that thymines point away from the helical axis of the G-quadruplex (*46*, *47*), implying that they do not contribute to the overall structure. Similarly, the NMR structure of $[d(T_4G_4)]_4$ in the presence of K^+ showed that the first three thymines of each strand were flexible and experienced multiple conformations (*45*); however, thymines directly adjacent to the 5′-guanine tetrad in $[d(T_4G_4)]_4$ maintained the right-handed helical structure (*45*). Thus, models of ligands bound to parallel-stranded G-quadruplexes do not include significant interactions between bound ligands and thymines. For example, for 1,4-bispiperidino amidoanthraquinone bound to $[d(TG_4T)]_4$, the diffraction pattern indicated six planar species in the structure, which were assigned to four guanine quartet planes and two ligand molecules (*3*). Subsequent molecular modeling determined that the energetically most favorable state contained one amidoanthraquinone molecule end-stacked on the 5′ side of the first guanine quartet and a second end-stacked on the 3′ side of the last guanine quartet (*3*). The crystal structure of daunomycin bound to $[d(TG_4T)]_4$ shows that a "daunomycin sandwich" forms between two molecules of $[d(TG_4T)]_4$: three coplanar daunomycin molecules stack externally at the 5′ end of two molecules of $[d(TG_4T)]_4$, which in turn are stacked 5′ end to 5′ end (*17*). The crystallization process most likely induces stacking to maximize hydrophobic contacts so that this structure might not represent the dominant solution species. Finally, two NMR-based models for *N*,*N*′-bis[2-(1-piperidino)ethyl]-3,4,9,10-perylenetetracarboxylic diimide (PIPER) binding to parallel-stranded G-quadruplexes have been proposed: one in which a molecule of PIPER is sandwiched between the 3′ ends of two molecules of $[d(TTAGGG)]_4$ and a second in which one PIPER molecule is bound between the guanine and the thymine in $[d(TAGGGTTA)]_4$ (*16*). All of these structures indicate that a reasonable model for CuTMpyP4 bound to $(\mathbf{1})_4$, a parallel-stranded G-quadruplex, should include end stacking of the porphyrin on the G-quadruplex.

Assuming that $(\mathbf{1})_4$ has a similar structure to $[d(TG_4T)]_4$ and given that we obtain a 2:1 binding stoichiometry for CuTMpyP4 bound to $(\mathbf{1})_4$, one molecule of CuTMpyP4 could be stacked at each end of the guanine stack in $(\mathbf{1})_4$. Our site size of four is consistent with this proposed location for the two CuTMpyP4 molecules in $(\mathbf{1})_4$. External binding of CuTMpyP4 in the grooves of $(\mathbf{1})_4$ is not expected because the parallel-stranded G-quadruplex formed by $d(TG_4T)$ has four nearly equivalent grooves that range in size from 2.2 to 3.3 Å (*47*). These grooves are significantly smaller than the minor groove of duplex DNA (*53*), which is where externally bound porphyrins reside (*54*). Because $(\mathbf{3})_4$ has twice as many stacks of guanines as $(\mathbf{1})_4$, a ligand might be able to intercalate into $(\mathbf{3})_4$ without significant disruption of the helix. In fact, Read and Neidle have suggested that "full" intercalation of a ligand into a quadruplex containing more than four consecutive guanine quartets might be possible (*3*). Therefore, we propose that, for the 3:1 binding stoichiometry of CuTMpyP4 to $(\mathbf{3})_4$, two molecules of CuTMpyP4 stack externally at ends of the guanine run and one molecule of CuTMpyP4 intercalates between guanine planes. Although other binding arrangements are possible, these suggested CuTMpyP4 binding locations are the most likely based on published drug−guanine quadruplex structures and our spectroscopic evidence.

The observation of an emission spectrum for CuTMpyP4 provides support for end stacking and/or intercalation into the G-quadruplexes. Emission spectra of CuTMpyP4 with mixed sequence DNA, poly(dG−dC)·poly(dG−dC), or poly(dA−dT)·poly(dA−dT) led Hudson et al. to conclude that intercalation prevents solvent quenching of the CuTMpyP4 excited state by protecting Cu^{2+} axial ligand-binding sites (*55*). We observe an emission spectrum for CuTMpyP4 with $(\mathbf{1})_4$ or $(\mathbf{3})_4$, indicating that CuTMpyP4 is protected from solvent. If two CuTMpyP4 molecules end stack on $(\mathbf{1})_4$, two of the total four Cu^{2+} axial ligand-binding sites would be protected from solvent by interaction with a plane of guanines. The other two Cu^{2+} axial ligand-binding sites would be partially protected from solvent by thymines. The ascribed role of partial protection from solvent by thymines is supported by the NMR model of $[d(T_4G_4)]_4$ showing that the thymines adjacent to the guanine quartet stack maintain the right-handed helical structure but that they are not as ordered as guanines in the neighboring guanine quartet (*45*). The net effect is that, for two CuTMpyP4 molecules bound per $(\mathbf{1})_4$, two Cu^{2+} axial ligand-binding sites are completely protected and two are partially protected from solvent,

leading to the observation of an emission spectrum for CuTMpyP4.

The emission intensity of CuTMpyP4 bound to $(\mathbf{3})_4$, which contains eight guanine quartets, is increased significantly over that observed for CuTMpyP4 bound to $(\mathbf{1})_4$, which contains four guanine quartets. This increased emission intensity is consistent with the report that CuTMpyP4 emission intensity increases as the GC content of DNA increases, thereby increasing the number of possible intercalation sites (*55*). By analogy, we ascribe the increased emission intensity of CuTMpyP4 bound to $(\mathbf{3})_4$ as compared to that for CuTMpyP4 bound to $(\mathbf{1})_4$ to increased protection of Cu^{2+} axial ligand-binding sites from solvent. Because we propose that both oligonucleotides have the same number of end-stacking sites (two per G-quadruplex), the increased emission intensity for CuTMpyP4 bound to $(\mathbf{3})_4$ can be ascribed tentatively to intercalation of one CuTMpyP4 between guanine quartet planes in the quadruplex. Two of the three CuTMpyP4 molecules bound to $(\mathbf{3})_4$ end stack on each end of the run of eight guanines. The third molecule of CuTMpyP4 would intercalate into $(\mathbf{3})_4$, a situation that protects both of its Cu^{2+} axial ligand-binding sites from the solvent, causing an increase in emission intensity for CuTMpyP4 bound to $(\mathbf{3})_4$ over that observed for CuTMpyP4 bound to $(\mathbf{1})_4$.

Similar conclusions regarding the CuTMpyP4-binding environment can be drawn from the EPR spectra. Both spectra for CuTMpyP4 with $(\mathbf{1})_4$ or $(\mathbf{3})_4$ show increased Cu−N superhyperfine coupling relative to CuTMpyP4 in buffer solution. The increase in the average Cu−N superhyperfine (A_N) coupling constant indicates a stronger interaction between the unpaired electron on Cu^{2+} [in a $d_{x^2-y^2}$ orbital (*41*, *56*)] and the nitrogen atoms of the porphyrin ring. The stronger coupling could be due to decreased flexibility of the porphyrin because of a more rigid environment in the presence of the oligonucleotides than in buffer solution. End stacking of CuTMpyP4 on the 5′- and 3′-guanine quartet planes in $(\mathbf{1})_4$ would restrict the mobility of CuTMpyP4 more than in buffer solution but to a lesser degree than end stacking plus intercalation in $(\mathbf{3})_4$.

A further piece of structural information derived from the EPR spectra is that CuTMpyP4 does not intercalate into adjacent G-quartet planes as suggested for H_2TMpyP4 by Haq et al. (*18*). If CuTMpyP4 molecules were intercalated into adjacent guanine quartet planes, the EPR spectra should show strong coupling (*24*, *25*, *31*) because the CuTMpyP4 molecules would be approximately 4 Å apart [on the basis of the average distance between Na^+ ions in the crystal structure of $[d(TG_4T)]_4$ (*47*)]. Distances of 3.5−4.0 Å between Cu^{2+} ions have been used to model spectra for dimeric porphyrin species (*24*, *25*). CuTMpyP4 does not dimerize in dilute solution (*31*, *49*, *57*, *58*), but it is possible that binding to the G-quadruplex could force Cu^{2+} ions into close proximity. However, no half-field transition ($\Delta m_s = \pm 2$) or spectral broadening is observed in EPR spectra of CuTMpyP4 with either $(\mathbf{1})_4$ or $(\mathbf{3})_4$, indicating that the CuTMpyP4 molecules are not spatially close.

Our model for CuTMpyP4 bound to the parallel-stranded G-quadruplexes formed by **1** and **3** is attractive because it is consistent with the spectroscopic properties of CuTMpyP4 with $(\mathbf{1})_4$ or $(\mathbf{3})_4$, the binding stoichiometries for CuTMpyP4 with $(\mathbf{1})_4$ and $(\mathbf{3})_4$, and known structures of parallel-stranded G-quadruplexes containing bound ligands. Attempts are underway to test this model using parallel-stranded G-quadruplexes with varying guanine contents. Confirmation of this model for CuTMpyP4 binding to G-quadruplexes would demonstrate that intercalation of a ligand *between* the guanine stacks of a G-quadruplex is possible, as proposed previously by others (*1*, *3*, *18*).

ACKNOWLEDGMENT

Critical reading of the manuscript by Dr. David H. Stewart is acknowledged.

SUPPORTING INFORMATION AVAILABLE

Absorption titrations, binding curves, Scatchard plots, *r* versus free CuTMpyP4 concentration plots of the Watson−Crick complementary strands of **1** and **3**, and the absorption difference spectra for **1** and **3** used to generate Job plots. This material is available free of charge via the Internet at http://pubs.acs.org.

REFERENCES

1. Anantha, N. V., Azam, N., and Sheardy, R. D. (1998) Porphyrin Binding to Quadruplexed T_4G_4, *Biochemistry 37*, 2709−2714.
2. Cech, T. (2000) Life at the End of the Chromosome: Telomeres and Telomerase, *Angew. Chem., Int. Ed. 39*, 34−43.
3. Read, M. A., and Neidle, S. (2000) Structural Characterization of a Guanine-Quadruplex Ligand Complex, *Biochemistry 39*, 13422−13432.
4. Vialas, C., Pratviel, G., and Meunier, B. (2000) Oxidative Damage Generated by an Oxo-metalloporphyrin onto the Human Telomeric Sequence, *Biochemistry 39*, 9514−9522.
5. Mergny, J.-L., Mailliet, P., Lavelle, F., Riou, J.-F., Lauoi, A., and Hélène, C. (1999) The Development of Telomerase Inhibitors: The G-Quartet Approach, *Anti-Cancer Drug Des. 14*, 327−339.
6. Izbicka, E., Wheelhouse, R. T., Raymond, E., Davidson, K. K., Lawrence, R. A., Sun, D., Windle, B. E., Hurley, L. H., and Von Hoff, D. D. (1999) Effects of Cationic Porphyrins as G-Quadruplex Interactive Agents in Human Tumor Cells, *Cancer Res. 59*, 639−644.
7. Neidle, S., and Parkinson, G. (2002) Telomere Maintenance as a Target for Anticancer Drug Discovery, *Nat. Rev. Drug Discovery 1*, 383−393.
8. Parkinson, G. N., Lee, M. P. H., and Neidle, S. (2002) Crystal Structure of Parallel Quadruplexes from Human Telomeric DNA, *Nature 417*, 876−880.
9. Han, H., Langley, D. R., Rangan, A., and Hurley, L. H. (2001) Selective Interactions of Cationic Porphyrins with G-Quadruplex Structures, *J. Am. Chem. Soc. 123*, 8902−8913.
10. Sun, D., Thompson, B., Cathers, B. E., Salazar, M., Kerwin, S. M., Trent, J. O., Jenkins, T. C., Neidle, S., and Hurley, L. H. (1997) Inhibition of Human Telomerase by a G-Quadruplex-Interactive Compound, *J. Med. Chem. 40*, 2113-2116.
11. Han, H., Bennett, R. J., and Hurley, L. H. (2000) Inhibition of Unwinding of G-Quadruplex Structures by Sgs1 Helicase in the Presence of *N*,*N*′-Bis[2-(1-piperidino)ethyl]3,4,9,10-perylenetetracarboxylic Diimide, a G-Quadruplex-Interactive Ligand, *Biochemistry 39*, 9311−9316.
12. Haider, S. M., Parkinson, G. N., and Neidle, S. (2003) Structure of a G-Quadruplex−Ligand Complex, *J. Mol. Biol. 326*, 117−125.
13. Shi, D., Wheelhouse, R. T., Sun, D., and Hurley, L. H. (2001) Quadruplex-Interactive Agents as Telomerase Inhibitors: Synthesis of Porphyrins and Structure−Activity Relationships for the Inhibition of Telomerase, *J. Med. Chem. 44*, 4509−4523.
14. Nakatani, K., Hagihara, S., Sando, S., Sakamoto, S., Yamaguchi, K., Maesawa, C., and Saito, I. (2003) Induction of a Remarkable Conformational Change in a Human Telomeric Sequence by the Binding of Naphthyridine Dimer: Inhibition of the Elongation of a Telomeric Repeat by Telomerase, *J. Am. Chem. Soc. 125*, 662−666.
15. Grand, C. L., Han, H., Munoz, R. M., Weitman, S., Von Hoff, D. D., Hurley, L. H., and Bearss, D. J. (2002) The Cationic Porphyrin TMPyP4 Down-Regulates *c-myc* and Human Telomerase Reverse

Transcriptase Expression and Inhibits Tumor Growth *in Vivo*, *Mol. Cancer Ther. 1*, 565−573.
16. Fedoroff, O. Y., Salazar, M., Han, H., Chemeris, V. V., Kerwin, S. M., and Hurley, L. H. (1998) NMR-Based Model of a Telomerase-Inhibiting Compound Bound to G-Quadruplex DNA, *Biochemistry 37*, 12367−12374.
17. Clark, G. R., Pytel, P. D., Squire, C. J., and Neidle, S. (2003) Structure of the First Parallel DNA Quadruplex−Drug Complex, *J. Am. Chem. Soc. 125*, 4066−4067.
18. Haq, I., Trent, J. O., Chowdhry, B. Z., and Jenkins, T. C. (1999) Intercalative G-Tetraplex Stabilization of Telomeric DNA by a Cationic Porphyrin, *J. Am. Chem. Soc. 121*, 1768−1779.
19. Han, F. X., Wheelhouse, R. T., and Hurley, L. H. (1999) Interactions of TMPyP4 and TMPyP2 with Quadruplex DNA. Structural Basis for the Differential Effects on Telomerase Inhibition, *J. Am. Chem. Soc. 121*, 3561−3570.
20. Wheelhouse, R. T., Sun, D., Han, H., Han, F. X., and Hurley, L. H. (1998) Cationic Porphyrins as Telomerase Inhibitors: The Interaction of Tetra-(*N*-methyl-4-pyridyl)porphine with quadruplex DNA, *J. Am. Chem. Soc. 120*, 3261−3262.
21. Kim, M.-Y., Vankayalapati, H., Shin-ya, K., Wierzba, K., and Hurley, L. H. (2002) Telemostatin, a Potent Telomerase Inhibitor that Interacts Quite Specifically with the Human Telomeric Intramolecular G-Quadruplex, *J. Am. Chem. Soc. 124*, 2098−2099.
22. Kim, M.-Y., Duan, W., Gleason-Guzman, M., and Hurley, L. H. (2003) Design, Synthesis, and Biological Evaluation of a Series of Fluoroquinoanthroxazines with Contrasting Dual Mechanisms of Action against Topoisomerase II and G-Quadruplexes, *J. Med. Chem. 46*, 571−583.
23. Uno, T., Aoki, K., Shikimi, T., Hiranuma, Y., Tomisugi, Y., and Ishikawa, Y. (2002) Copper Insertion Facilitates Water-Soluble Porphyrin Binding to rA-rU and rA-rT Base Pairs in Duplex RNA and RNA-DNA Hybrids, *Biochemistry 41*, 13059−13066.
24. Blumberg, W. E., and Peisach, J. (1965) An Electron Spin Resonance Study of Copper Uroporphyrin III and Other Touraco Feather Components, *J. Biol. Chem. 240*, 870−876.
25. Eaton, S. S., Eaton, G. R., and Chang, C. K. (1985) Synthesis and Geometry Determination of Cofacial Diporphyrins. EPR Spectroscopy of Dicopper Diporphyrins in Frozen Solution, *J. Am. Chem. Soc. 107*, 3177−3184.
26. Pasternack, R. F., and Gibbs, E. J. (1989) Interaction of Porphyrins and Metalloporphyrins with Nucleic Acids, in *Metal−DNA Chemistry* (Tullius, T., Ed.) pp 59−73, American Chemical Society, Washington, DC.
27. Pasternack, R. F., Gibbs, E. J., and Villafranca, J. J. (1983) Interactions of Porphyrins with Nucleic Acids, *Biochemistry 22*, 2406−2414.
28. Sambrook, J., and Russell, D. (2001) *Molecular Cloning A Laboratory Manual*, Vol. 2, 3rd ed., Cold Spring Harbor Laboratory Press, Cold Spring Harbor, NY.
29. Fasman, G. (1975) *Handbook of Biochemistry and Molecular Biology*, CRC Press, Cleveland, OH.
30. Peacocke, A. R., and Skerrett, J. N. H. (1956) The Interaction of Aminoacridines with Nucleic Acids, *Trans. Faraday Soc. 52*, 261−269.
31. Dougherty, G., and Pasternack, R. F. (1992) Aggregation of Copper(II) Derivatives of meso-Substituted Porphyrins in Frozen Aqueous Media, *Inorg. Chim. Acta 195*, 95−100.
32. Keniry, M. A. (2001) Quadruplex Structures in Nucleic Acids, *Biopolymers 56*, 123−146.
33. Gray, D. M., Ratliff, R. L., and Vaughan, M. R. (1992) Circular Dichroism Spectroscopy of DNA, *Methods Enzymol. 211*, 389−406.
34. Kowalczykowski, S., Leland, S., Lonberg, N., Newport, J., McSwiggen, J., and von Hippel, P. H. (1986) Cooperative and Noncooperative Binding of Protein Ligands to Nucleic Acid Lattices: Experimental Approaches to the Determination of Thermodynamic Parameters, *Biochemistry 25*, 1226−1240.
35. Cantor, C. R., and Schimmel, P. R. (1980) *Biophysical Chemistry*, Vol. 2, W. H. Freeman, San Francisco, CA.
36. van Holde, K. E., Johnson, W. C., and Ho, P. S. (1998) *Principles of Biophysical Chemistry*, Prentice Hall, Upper Saddle River, NJ.
37. *NFIT* (1990) The University of Texas, Galveston, TX.
38. McGhee, J. D., and von Hippel, P. H. (1974) Theoretical Aspects of DNA−Protein Interactions: Co-operative and Non-co-operative Binding of Large Ligands to a One-Dimensional Homogeneous Lattice, *J. Mol. Biol. 86*, 469−489.
39. Chaires, J. B. (2001) Analysis and Interpretation of Ligand−DNA Binding Isotherms, *Methods Enzymol. 340*, 3−22.
40. Horton, T. E., Clardy, D. R., and DeRose, V. J. (1998) Electron Paramagnetic Resonance Spectroscopic Measurement of Mn^{2+} Binding Affinities to the Hammerhead Ribozyme and Correlation with Cleavage Activity, *Biochemistry 37*, 18094−18101.
41. Subramanian, J. (1975) Electron Paramagnetic Resonance Spectroscopy of Porphyrins and Metalloporphyrins, in *Porphyrins and Metalloporphyrins* (Smith, K. M., Ed.) pp 555−589, Elsevier, Amsterdam, The Netherlands.
42. Greiner, S. P., Rowlands, D. L., and Kreilick, R. W. (1992) EPR and ENDOR Study of Selected Porphyrin− and Phthalocyanine−Copper Complexes, *J. Phys. Chem. 96*, 9132−9139.
43. Dougherty, G., Pilbrow, J. R., Skorobogaty, A., and Smith, T. D. (1985) Electron Spin Resonance Spectroscopic and Spectrophotometric Investigation of the Binding of Tetracationic Porphryins and Porphyrazines with Calf Thymus DNA, *J. Chem. Soc., Faraday Trans. 81*, 1739−1759.
44. Dougherty, G. (1988) Intercalation of Tetracationic Metalloporphyrins and Related Compounds into DNA, *J. Inorg. Biochem. 34*, 95−103.
45. Gupta, G., Garcia, A. E., Guo, Q., Lu, M., and Kallenbach, N. R. (1993) Structure of a Parallel-Stranded Tetramer of the Oxytricha Telomeric DNA Sequence of dT_4G_4, *Biochemistry 32*, 7098−7103.
46. Laughlan, G., Murchie, A. I. H., Norman, D. G., Moore, M. H., Moody, P. C. E., Lilley, D. M. J., and Luisi, B. (1994) The High-Resolution Crystal Structure of a Parallel-Stranded Guanine Tetraplex, *Science 265*, 520−524.
47. Phillips, K., Dauter, Z., Murchie, A. I. H., Lilley, D. M. J., and Luisi, B. (1997) The Crystal Structure of a Parallel-Stranded Guanine Tetraplex at 0.95 Å Resolution, *J. Mol. Biol. 273*, 171−182.
48. Read, M. A., Wood, A. A., Harrison, J. R., Gowan, S. M., Kelland, L. R., Dosanjh, H. S., and Neidle, S. (1999) Molecular Modeling Studies on G-Quadruplex Complexes of Telomerase Inhibitors: Structure−Activity Relationships, *J. Med. Chem. 42*, 4538−4546.
49. Pasternack, R. F., Gibbs, E. J., Gaudemer, A., Antebi, A., Bassner, S., DePoy, L., Turner, D. H., Williams, A., Laplace, F., Lansard, M. H., Merienne, C., and Perree-Fauvet, M. (1985) Molecular Complexes of Nucleosides and Nucleotides with a Monomeric Cationic Porphyrin and Some of its Metal Derivatives, *J. Am. Chem. Soc. 107*, 8179−8186.
50. Musier, K. M., and Hammes, G. G. (1988) Assessment of the Number of Nucleotide Binding Sites on Chloroplast Coupling Factor 1 by the Continuous Variation Method, *Biochemistry 27*, 7015−7020.
51. Ingham, K. C. (1975) On the Application of Job's Method of Continuous Variation to the Stoichiometry of Protein−Ligand Complexes, *Anal. Biochem. 68*, 660−663.
52. Huang, C. Y. (1982) Determination of Binding Stoichiometry by the Continuous Variation Method: The Job Plot, *Methods Enzymol. 87*, 509−525.
53. Bloomfield, V. A., Crothers, D. M., and Tinoco, I. J. (2000) *Nucleic Acids Structures, Properties, and Functions*, University Science Books, Sausalito, CA.
54. Pasternack, R. F., and Gibbs, E. J. (1996) Porphyrin and Metalloporphyrin Interactions with Nucleic Acids, in *Metal Ions in Biological Systems* (Sigel, A., and Sigel, H., Eds.) pp 367−397, Marcel Dekker, Inc., New York.
55. Hudson, B. P., Sou, J., Berger, D. J., and McMillin, D. R. (1992) Luminescence Studies of the Intercalation of Cu(TMpyP4) into DNA, *J. Am. Chem. Soc. 114*, 8997−9002.
56. Walker, F. A. (2000) Proton NMR and EPR Spectroscopy of Paramagnetic Metalloporphyrins, in *The Porphyrin Handbook* (Kadish, K. M., Smith, K. M., and Guilard, R., Eds.) pp 81−183, Academic Press, San Diego, CA.
57. Pasternack, R. F., Francesconi, L., Raff, J., and Spiro, E. (1973) Aggregation of Nickel(II), Copper(II), and Zinc(II) Derivatives of Water-Soluble Porphyrins, *Inorg. Chem. 12*, 2606−2611.
58. Pasternack, R. F., Huber, P. R., Boyd, P. D. W., Engasser, G., Francesconi, L., Gibbs, E. J., Fasella, P., Venturo, G. C., and Hinds, L. deC. (1972) On the Aggregation of Meso-Substituted Water-Soluble Porphryins, *J. Am. Chem. Soc. 94*, 4511−4517.

BI0483209